Am J Physiol Endocrinol Metab 297: E438–E451, 2009.
First published May 12, 2009; doi:10.1152/ajpendo.90784.2008.

Role of caveolin-1 in thyroid phenotype, cell homeostasis, and hormone synthesis: in vivo study of caveolin-1 knockout mice

Maximin Senou,[1]* Maria José Costa,[5]* Claude Massart,[5] Matthieu Thimmesch,[1] Céline Khalifa,[1] Sylvie Poncin,[1] Marie Boucquey,[1] Anne-Catherine Gérard,[1] Jean-Nicolas Audinot,[6] Chantal Dessy,[2] Jean Ruf,[7] Olivier Feron,[2] Olivier Devuyst,[3] Yves Guiot,[4] Jacques Emile Dumont,[5] Jacqueline Van Sande,[5] and Marie-Christine Many[1]

[1]*Unité de Morphologie Expérimentale,* [2]*Unité de Pharmacothérapie,* [3]*Unité de Néphrologie,* [4]*Département de Pathologie, Université Catholique de Louvain;* [5]*Institut de Recherche Interdisciplinaire, Université Libre de Bruxelles, Brussels, Belgium;* [6]*Laboratoire d'Analyse des Matériaux, Centre de Recherche Public Gabriel Lippmann, Luxembourg; and* [7]*Université de la Méditerranée, Marseille, France*

Submitted 17 April 2008; accepted in final form 6 May 2009

Senou M, Costa MJ, Massart C, Thimmesch M, Khalifa C, Poncin S, Boucquey M, Gérard A, Audinot J, Dessy C, Ruf J, Feron O, Devuyst O, Guiot Y, Dumont JE, Van Sande J, Many MC. Role of caveolin-1 in thyroid phenotype, cell homeostasis, and hormone synthesis: in vivo study of caveolin-1 knockout mice. *Am J Physiol Endocrinol Metab* 297: E438–E451, 2009. First published May 12, 2009; doi:10.1152/ajpendo.90784.2008.—In human thyroid, caveolin-1 is localized at the apex of thyrocytes, but its role there remains unknown. Using immunohistochemistry, ^{127}I imaging, transmission electron microscopy, immunogold electron microscopy, and quantification of H_2O_2, we found that in caveolin-1 knockout mice thyroid cell homeostasis was disrupted, with evidence of oxidative stress, cell damage, and apoptosis. An even more striking phenotype was the absence of thyroglobulin and iodine in one-half of the follicular lumina and their presence in the cytosol, suggesting that the iodide organification and binding to thyroglobulin were intracellular rather than at the apical membrane/extracellular colloid interface. The latter abnormality may be secondary to the observed mislocalization of the thyroid hormone synthesis machinery (dual oxidases, thyroperoxidase) in the cytosol. Nevertheless, the overall uptake of radioiodide, its organification, and secretion as thyroid hormones were comparable to those of wild-type mice, suggesting adequate compensation by the normal TSH retrocontrol. Accordingly, the levels of free thyroxine and TSH were normal. Only the levels of free triiodothyronine showed a slight decrease in caveolin-1 knockout mice. However, when TSH levels were increased through low-iodine chow and sodium perchlorate, the induced goiter was more prominent in caveolin-1 knockout mice. We conclude that caveolin-1 plays a role in proper thyroid hormone synthesis as well as in cell number homeostasis. Our study demonstrates for the first time a physiological function of caveolin-1 in the thyroid gland. Because the expression and subcellular localization of caveolin-1 were similar between normal human and murine thyroids, our findings in caveolin-1 knockout mice may have direct relevance to the human counterpart.

dual oxidase; thyroperoxidase; iodination; thyrocytes; hydrogen peroxide; oxidative stress; thyroid hormone synthesis; iodide

CAVEOLAE WERE FIRST DESCRIBED in the early 1950s by Palade (38) and Yamada (61) at the surface of endothelial and epithelial cells, respectively. They are invaginated microdomains of the plasma membrane found in diverse cell types: adipocytes, endothelial and epithelial cells, myocytes, and fibroblasts (31). The formation of caveolae is the result of a local accumulation of glycosphingolipids, cholesterol, and caveolins in the membrane of the vesicles budding from the *trans*-Golgi network (40). The discovery of caveolins is much more recent (33, 51). Caveolins are the protein markers of caveolae, and they are intricately involved in caveolar functioning. There are three different caveolin proteins: caveolin-1 (Cav-1) and caveolin-2 are coexpressed and colocalized in numerous cell types, whereas the expression of caveolin-3 is specific to cardiac, skeletal, and smooth muscle cells (47). Both caveolins and caveolae appear to be multifunctional, and their specific role in a given cell type is often related to the particular function of that cell. The generation and analysis of Cav-1 knockout (Cav-$1^{-/-}$) mice undoubtedly demonstrated that Cav-1 is necessary for the biogenesis of caveolae and for the stabilization of the caveolin-2 protein (19, 45). Although viable, fertile, and apparently healthy, Cav-$1^{-/-}$ mice display several aberrant phenotypes that result in physical limitations. The most prominent phenotypes described so far are cardiovascular and pulmonary abnormalities due to impaired regulation of nitric oxide and calcium signaling and to the thickening of alveolar septa caused by hyperproliferation of endothelial cells and fibroblasts. As Cav-$1^{-/-}$ mice age, other phenotypes become apparent. They are leaner than wild-type littermates, due to deficient insulin receptor-mediated signaling in adipocytes (46), and have reduced life span as a consequence of the above-referred cardiovascular defects and heart hypertrophy (39).

Thyrocytes are polarized cells in which the synthesis of thyroid hormones takes place at the apical membrane-colloid interface and involves two enzymatic systems: dual oxidase (Duox) and thyroperoxidase (TPO). Duox generates the H_2O_2 (2, 3) needed to oxidize and activate the heme catalytic site of TPO. Once activated, TPO oxidizes iodide and iodinates tyrosine residues of Tg to form monoiodotyrosyls and diiodotyrosyls. TPO further couples the iodotyrosyls residues in thyroglobulin (Tg), resulting in the formation of triiodothyronine (T_3) and thyroxine (T_4).

Because Cav-1 is a putative tumor suppressor in human thyroid cells (2, 3), the analysis of the thyroid of Cav-$1^{-/-}$ mice is of particular interest. Indeed, we have previously demonstrated that Cav-1 acts as a negative regulator of proliferation in vivo (14). However, we also found that apoptosis is increased in the thyroid of Cav-$1^{-/-}$ mice, although the explanation for this remains unknown. We have observed that

* M. Senou and M. J. Costa contributed equally to this work.
Address for reprint requests and other correspondence: M.-C. Many, Unité de Morphologie Expérimentale, Université Catholique de Louvain, Brussels, Belgium (E-mail: Marie-Christine.Many@uclouvain.be).

normal human thyrocytes express high levels of Cav-1 and that this protein is localized mainly in the apical region of these cells (13). Altogether, these findings led us to the hypothesis that Cav-1 and, possibly, caveolae might play a role in the synthesis of thyroid hormones and in the homeostasis/survival of thyroid cells. Here, we investigated the specific role played by Cav-1 in the functioning of thyrocytes through a comparative analysis of the thyroids of control and Cav-$1^{-/-}$ mice. We show evidence that Cav-1 in thyroid is required for proper cell functioning and homeostasis.

MATERIALS AND METHODS

Animals and treatments. All procedures respected regulations and guidelines of the Belgian state and European Union and were approved by the local ethics committee. Cav-$1^{-/-}$ mice [strain no. 004585 (45)] were purchased from Jackson Laboratories.

In all experiments, the control mice used were the wild-type (WT) littermates of Cav-$1^{-/-}$ mice. The mice were kept in the animal facility under the 12:12-h dark-light cycle and were given water and AO3 mouse breeding diet (Safe UAR) with normal iodine content (0.4 mg/kg). For goiter induction, mice were fed a low-iodine diet (20 μg/kg; Animalabo, Brussels, Belgium) and received water containing $NaClO_4$ (1%) for 12 days.

Thyroid histology and staining of glycoproteins. Mice were euthanized, and the thyroids were removed, weighed, fixed in buffered-formalin, and embedded in paraffin. Thyroid sections (5 μm) were mounted on glass slides, deparaffinated, and hydrated. For histological analysis, sections were stained with hematoxylin and eosin (H&E), following a standard protocol. Glycoproteins were detected using Periodic Acid-Schiff staining (PAS). Sections were stained with 0.5% periodic acid for 30 min and with Schiff's reagent for 20 min and then rinsed in running tap water for 5 min. Nuclei were counterstained with hematoxylin for 3 min. Sections were rinsed in running tap water, dehydrated, cleared, and mounted.

Immunohistochemistry. Duox was detected on frozen sections. All the other proteins and 4-hydroxynonenal (HNE) were detected on paraffin sections. The sections for detection of Cav-1, Cav-2, HNE, and catalase were subjected to microwave pretreatment. The conditions of the staining are summarized in table 1. Negative controls included the replacement of primary antibody by the preimmune serum or absence of the primary antibody.

Transmission electron microscopy. Thyroid lobes were fixed in 2.5% glutaraldehyde in 0.1 M cacodylate buffer for 1.5 h, post-fixed in 1% osmium tetroxide for 1 h, and embedded in LX112 resin (Ladd Research Industries, Burlington, VT). Thin sections (0.5 μm) were stained with toluidine blue and analyzed for morphology by light microscopy. Ultrathin sections were prepared and stained with uranyl acetate and lead citrate and examined with an electron microscope Zeiss EM169 (Carl Zeiss, Oberkochem, Germany).

Ultrastructural distribution of iodide. Thyroid lobes were fixed in 2.5% glutaraldehyde in 0.1 M cacodylate buffer for 1.5 h and embedded in LX112 resin. Semi-thin sections were prepared, and the ultrastructural distribution of the iodide natural isotope (^{127}I) was obtained through imaging by SIMS (secondary ion mass spectrometry), using the NanoSIMS 50 system (5, 10, 27, 28, 42). Maps were acquired under standard analytic conditions: a Cs^+ primary beam with impact energy of 16 keV and a probe with current intensity of 1 pA. The analyzed surface was 30 × 30 μm. Under these conditions, a lateral resolution of 100 nm is expected. The detection of this element was done in the multicollection mode with parallel detection of ^{31}P, ^{12}C, ^{14}N, and ^{34}S. All images were acquired in 256 × 256 pixels with a counting time of 20 ms per pixel.

Immunogold electron microscopy. After rinses in PBS-BSA (1%), ultrathin sections (0.1 μm) were incubated overnight with a rabbit polyclonal anti-thyroglobulin antibody (1/300, DAKO). Then, they were rinsed and incubated for 30 min with a 12-nm colloidal gold affinity pure goat anti-rabbit IgG (Jackson, 111-205-144, lot no. 71647). Sections were postfixed with 2.5% glutaraldehyde for 5 min and counterstained. They were examined with a Zeiss 109 transmission electron microscope. Negative control is obtained by omission of primary antibody, and the colloid of Cav-$1^{+/+}$ follicles served as positive control.

Serum free T_3 and free T_4 assay. The free thyroid hormone levels in sera were measured by a competitive assay using chemiluminescence (module E170, Roche Diagnostics, Mannheim, Germany).

Bioassay of TSH. TSH was evaluated by bioassay using a line of Chinese hamster ovary cells (CHO-K1) stably transfected with a human TSH receptor cDNA, as previously described (41). Briefly, 50,000 cells were seeded in individual test tubes and incubated for 24 h in 100 μl of Ham's F-12 cell culture medium supplemented with 10% fetal calf serum, 100 IU/ml penicillin, 100 μg/ml streptomycin, 1 mM sodium pyruvate, and 2.5 μg/ml Fungizone. Cells were washed with 500 μl of Krebs-Ringer-HEPES buffer (pH 7.4) supplemented with 8 mM glucose and 0.5 g/l BSA and then preincubated for 30 min in 200 μl of the same medium. The medium was removed, and 200 μl of fresh medium containing 20 μl of serum for TSH measurement and 25 μM Rolipram, a cAMP phosphodiesterase inhibitor, was added. After a 1-h incubation, the medium was discarded and replaced with 1 ml of 0.1 M HCl. cAMP was measured in the dried cell extract by RIA according to the method of Brooker (9). Values obtained with CHO-K1 cells devoid of TSH receptor were considered as blanks. Results are expressed as means ± SD. Bioassays of TSH were validated by RIA (44).

In vivo iodide uptake and in vitro secretion. The mice received an intraperitoneal injection of 30 μCi $^{125}I^-$ the day before the experiment. The trachea and thyroids removed en bloc were preincubated for 1 h and incubated for 3 h in 2 ml of Krebs-Ringer-bicarbonate medium supplemented with 8 mM glucose, 0.5 g/l BSA, and 10^{-4} M $NaClO_4$ plus 10^{-4} M methimazole to avoid iodide recirculation. TSH (5 mU/ml) was added at the start of the incubation. The butanol extraction, which contains the thyroid hormones, was performed as previously described (56). The iodide uptake in vivo is expressed as counts per minute per trachea. The secretion is expressed as a percentage of the total radioactivity in the tissue at the beginning of the incubation ($BE^{125}I$, the residual pellet and the tissue).

In vitro $PB^{125}I$ (iodide organification). Thyroid lobes were dissected and preincubated for 1 h in 2 ml of Krebs-Ringer-bicarbonate buffer supplemented with 8 mM glucose and 0.5 g/l BSA. Then, the tissue was transferred to fresh medium containing 7.10^{-6} M KI and 2

Table 1. *Experimental conditions for immunohistochemistry*

Protein	Primary Antibody	Incubation Conditions
Cav-1	Rabbit polyclonal antibody (BD Transduction Laboratories)	625 ng/ml, 3 h
Cav-2	Mouse monoclonal antibody (BD Transduction Laboratories)	62 ng/ml, 3 h
Tg	Rabbit polyclonal antibody (Dako)	diluted 1/1,500, overnight
Tg-I	Mouse monoclonal antibody (B1) (17)	diluted 1/3,000, overnight
Duox	Rabbit polyclonal antibody (16)	diluted 1/3,000, overnight
TPO	Rabbit antibody Loœd TPO 821 (52)	4 μg/ml, 3 h
HNE	Rabbit polyclonal antibody (Calbiochem)	5 μg/ml, 1 h
PRDX5	Rabbit polyclonal antibody (57)	2.5 μg/ml, 3 h
Catalase	Mouse monoclonal antibody (Sigma)	11 μg/ml, 3 h

Cav, caveolin; Tg,; Tg-I, Thyroxine-rich Tg; Duox, dual oxidase; TPO, thyroperoxidase; HNE, 4-hydroxynonenal; PRDX5, peroxiredoxin 5. Nos. in parentheses are of references.

μCi/ml $^{125}I^-$. TSH (10 mU/ml) was added at the beginning of the incubation (2 h). Protein iodination was measured as described previously (50). Results are expressed as the percentage of the total radioactivity incorporated in the tissue.

H_2O_2 determination. Carefully dissected thyroid lobes cut in two were preincubated for 30 min in 1 ml of Krebs-Ringer-HEPES medium supplemented with 8 mM glucose and 0.5 g/l BSA and then transferred to 600 μl of fresh medium containing 0.1 mg/ml horse-

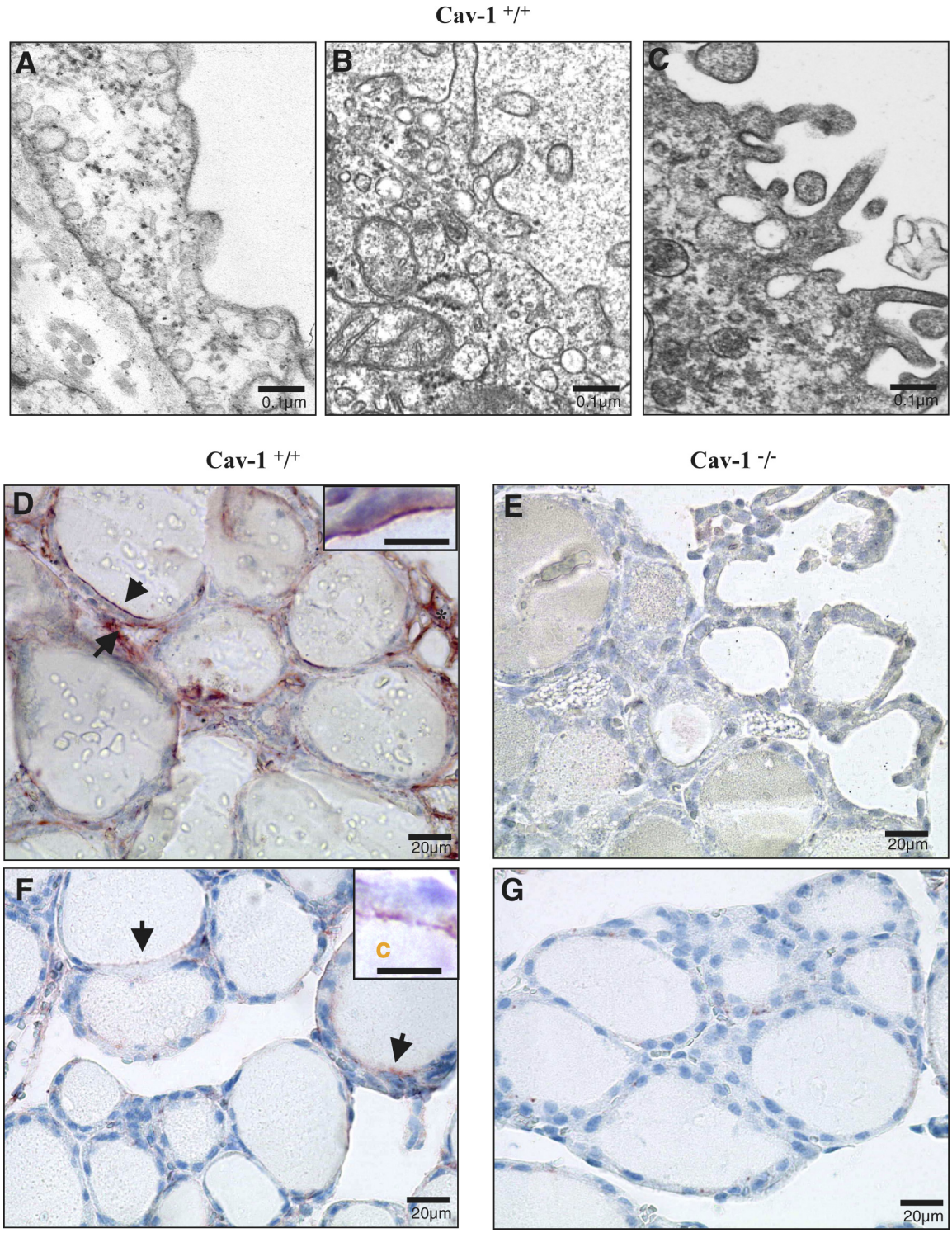

Fig. 1. A–C: transmission electron microscopy (TEM) micrographs of caveolin-1 wild-type (WT, Cav-$1^{+/+}$) thyroids. *A*: typical caveolae are observed in endothelial cells. *B* and *C*: similar caveolae are located at the apical pole of thyroid cells between the microvilli. *D–G*: thyroid sections (5 μm thick) from Cav-$1^{+/+}$ (*D–F*) and Cav-$1^{-/-}$ (*E–G*) mice. *D* and *E*: immunodetection of Cav-1. In WT mice (*D*), Cav-1 is detected at the apical pole of some thyrocytes (short arrow), on endothelial cells (long arrow), and on adipocytes (*), and it is not expressed in Cav-$1^{-/-}$ mice (*E*). *Inset*: Cav-1 localization at the apical pole facing the colloid (c) (bar, 10 μm). *F* and *G*: immunodetection of Cav-2. In WT mice (*D*), Cav-2 is also detected at the apical pole of thyrocytes (arrows; *inset*: bar, 10 μm). Its expression is lost in Cav-$1^{-/-}$ mice (*G*).

radish peroxidase type II, 440 μM homovanillic acid, with or without 10 mU/ml TSH. The fluorescence of the medium was measured 3 h later (315 and 425 nm excitation and emission wavelengths, respectively) (7).

Reproducibility. In qualitative experiments, one representative result is shown. In quantitative experiments, differences between WT and Cav-1$^{-/-}$ mice were analyzed using the Student's *t*-test. $P < 0.05$ was considered significant.

RESULTS

Validation of the Cav-1$^{-/-}$ mouse as a relevant animal model to study the role of Cav-1 in human thyroid. In previous studies, we (13) showed that Cav-1 expression pattern in thyroid follicular cells is heterogeneous and that the protein is localized mainly at the apical pole of follicular cells. To assess whether the study of Cav-1$^{-/-}$ mice would be relevant to understanding the role of Cav-1 in the human thyroid, we analyzed the existence of caveolae in the thyroid cells of mice, and we perfomed immunohistochemistry on the thyroids of control mice (WT littermates of Cav-1$^{-/-}$ mice) using the same antibody that we had used to detect Cav-1 in human samples. Caveolae have been extensively described in endothelial cells in different organs. They were also observed in the thyroid (Fig. 1*A*). Similar caveolae were detected in thyrocytes at the apical pole between microvilli (Fig. 1, *B* and *C*). By immunohistochemistry, we found that the Cav-1 staining pattern in the murine thyroid was similar to that found in the human thyroid (Fig. 1*D*). It was expressed at the apical pole of the thyrocytes (Fig. 1*D*, *inset*) as well as in endothelial cells and adipocytes. This similarity suggests that the murine thyroid may be a valid model of the human thyroid to study the role of Cav-1 in this organ. As expected, Cav-1 expression was not detected in the thyroid of Cav-1$^{-/-}$ mice (Fig. 1*E*).

Cav-2, like Cav-1, was located at the apical pole of thyrocytes in normal thyroids and was absent in the thyrocytes of Cav-1$^{-/-}$ mice (Fig. 1, *F* and *G*). As shown previously in vitro (14), Cav-1 expression was decreased in our perchlorate-stimulated glands (see Fig. 9, *A* and *B*).

The thyroid of Cav-1$^{-/-}$ mice displays histological abnormalities and deficient luminal storage of glycoproteins. We first looked roughly at dissection for obvious thyroid dysfunction in Cav-1$^{-/-}$ mice, but no visible goiter was observed. The mean thyroid weight was 3.7 ± 0.35 mg in Cav-1$^{-/-}$ mice and not significantly modified compared with Cav-1$^{+/+}$ mice. After the thyroids were removed, no differences were found in the thyroidal radioiodide uptake between WT and Cav-1$^{-/-}$ mice 24 h after an intraperitoneal injection of Na^{125}I (table 2).

We next searched for histological phenotypes in the thyroids of 2.5-mo-old Cav-1$^{-/-}$ mice. Thyroid sections from the same WT and Cav-1$^{-/-}$ samples used in Fig. 1, *D–G* were subjected to H&E staining. The absence of Cav-1 did not cause visible hyperplasia, and no signs of tumor induction were seen. Instead, compared with WT (Fig. 2*A*), we detected an absence of eosin staining in the lumina of many Cav-1$^{-/-}$ follicles (Fig. 2*B*). These follicles had a fragile appearance with rupture of the epithelial layer, and the follicular cells were square shaped, suggesting high secretory activity.

Table 2. *24-h thyroidal $^{125}I^-$ uptake in vivo*

	×10^6 cpm per Thyroid	*n*
WT	2.6±0.5	12
Cav-1$^{-/-}$	1.9±0.3	12
P	NS	

WT, wild type; NS, no statistically significant difference.

To determine whether the abnormal follicular lumina in Cav-1$^{-/-}$ thyroids lack glycoproteins, we performed PAS staining on sections of Cav-1$^{-/-}$ (Fig. 2*D*) and WT (Fig. 2*C*) thyroids. Again, many follicles showed no staining. The proportion of follicular lumina that were not PAS stained and therefore lacked glycosylated proteins was 45.8 ± 2.8% in Cav-1$^{-/-}$ mice vs. 3.8 ± 0.7% in WT (mean ± SE; $n = 7$ mice per group).

Absence of Cav-1 leads to defects in transport of the thyroid hormone synthesis machinery to the apical membrane. Since 45.8% of Cav-1$^{-/-}$ follicular lumina were not PAS stained and the colloid is >95% composed of the glycoprotein Tg, we speculated that Tg would be absent from those Cav-1$^{-/-}$ lumina. We analyzed Tg distribution by immunohistochemistry using two different antibodies: one that detects total Tg and another that recognizes only the T_4-rich Tg (Tg-I). In accord with the results obtained by H&E and PAS staining, we observed a similar proportion of Cav-1$^{-/-}$ follicles showing a lack of Tg in their lumina (Fig. 2*F* vs. control in 2*E*). These lumina of course failed to be stained by the antibody that specifically recognizes Tg-I (Fig. 2*H* vs. control in 2*G*). Furthermore, we noticed an accumulation of Tg and Tg-I in the apical region of the follicular cells in the abnormal Cav-1$^{-/-}$ follicles (Fig. 2, *F–H*).

The immunohistochemistry results suggest that Cav-1$^{-/-}$ thyrocytes have problems of Tg transport and luminal storage. This was also analyzed on semi-thin sections (Fig. 3 *A* and *B*) and transmission electron microscopy (TEM) (Fig. 3, *C* and *D*) on WT and Cav-1$^{-/-}$ thyroids. Contrary to WT (Fig. 3, *A* and *C*), we observed an accumulation of intracellular vesicles (Fig. 3*B*) and a remarkable distension of the rough endoplasmic reticulum (Fig. 3*D*), suggesting that Cav-1$^{-/-}$ thyrocytes have defects in the transport of newly synthesized proteins. The converse hypothesis, that this accumulation is due to defects in the postendocytotic processes, is very unlikely, as this would also lead to colloid accumulation in the lumen as it occurs in the quiescent thyroid follicles. Moreover, the dilatation of the ergastoplasm and the absence of real colloid droplets also suggest otherwise.

Absence of Cav-1 causes intracellular iodination. Does iodine also accumulate in the cells instead of being stored in the colloid of Cav-1$^{-/-}$ follicles? To address this question, we performed imaging by SIMS, a highly sensitive isotopic imaging technique uniquely suited for the study of trace ions distribution at the ultrastructural level. We therefore examined the distribution of the natural isotope ^{127}I in the thyroids of WT and Cav-1$^{-/-}$ mice using this method. As expected, ^{127}I was found in the follicular lumina of WT thyroids (Fig. 3*E*). In contrast, in Cav-1$^{-/-}$ mice, some lumina were devoided of ^{127}I (Fig. 3*F*). ^{127}I was detected in the cytoplasm of thyrocytes and on the apical membrane (Fig. 3*F*). This result confirmed the above-referred localization of Tg-I in the cytoplasm of thyrocytes. In fact, ^{127}I was detected in the cytoplasm of nearly all thyroid cells of Cav-1$^{-/-}$ mice. There were large and numerous intracytoplasmic vesicles filled with ^{127}I, these areas corresponding to dilated cisternae of endoplasmic reticulum

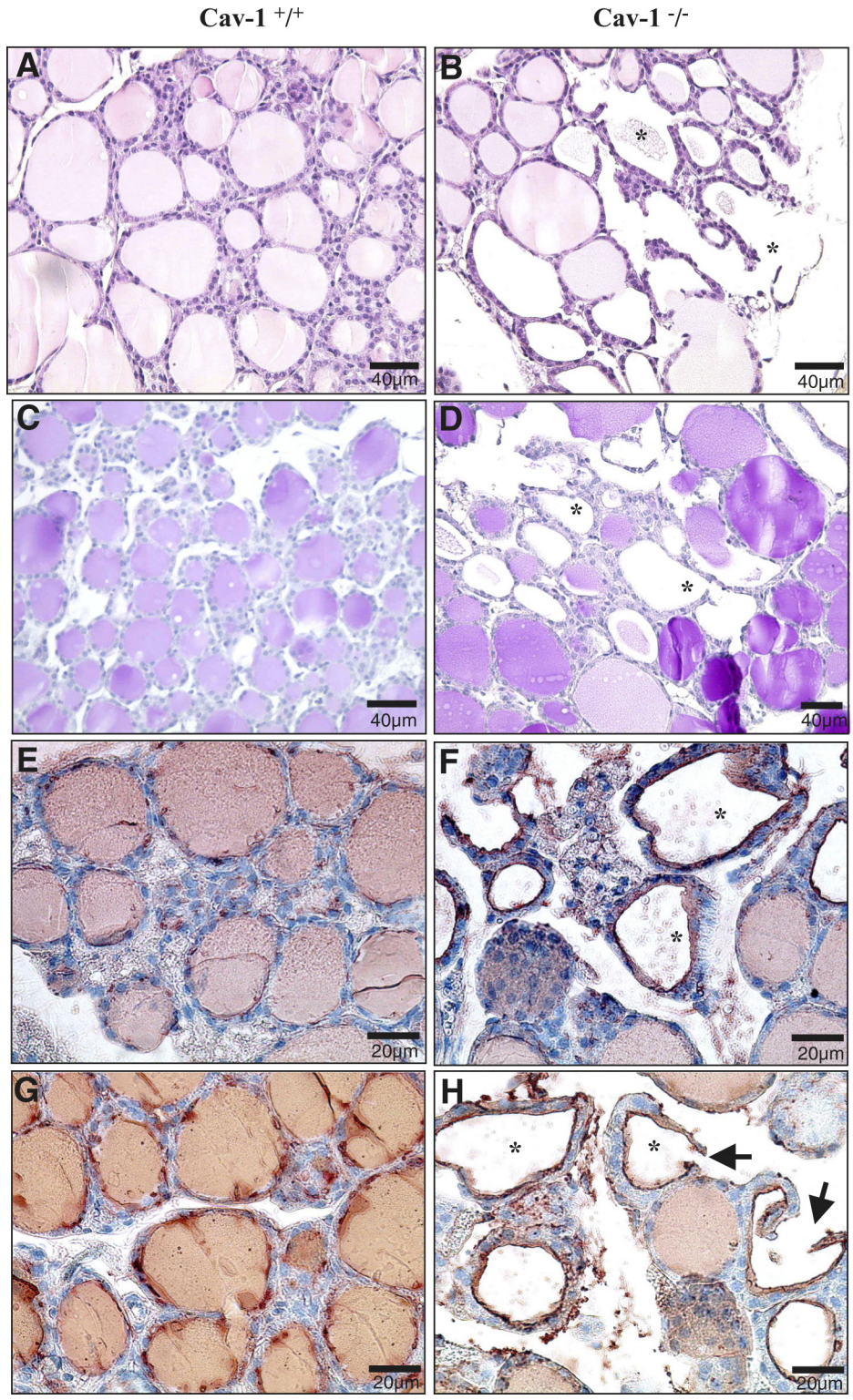

Fig. 2. Thyroid sections (5 μm thick) from Cav-$1^{+/+}$ (*A, C, E, G*) and Cav-$1^{-/-}$ (*B, D, F, H*) mice. *A* and *B*: H&E staining. *B*: in Cav-$1^{-/-}$ mice, some follicles (*) have an irregular outline, with an empty lumen surrounded by cylindrical cells. *C and D*: PAS staining. *D*: in Cav-$1^{-/-}$ mice, lumina of empty follicles (*) do not contain glycoproteins. *E and F*: immunodection of Tg. *G* and *H*: immunodetection of T_4-rich Tg (Tg-I). In Cav-$1^{-/-}$ mice, lumina of some follicles (*) do not contain Tg or Tg-I, which are instead detected in the cytoplasm and at the apical pole. Note the epithelial rupture of these altered follicles (arrows).

(Fig. 3, *G* and *H*). This was evidenced by immunogold labeling of Tg in electron microscopy. In Cav-$1^{+/+}$ follicles, Tg was detected in the colloid (Fig. 4*B*) compared with a specificity control of the immunolabeling obtained in the absence of the first antibody (Fig. 4*A*). In Cav-$1^{-/-}$ mice, Tg was absent in some lumina and detected in large dilatations of the rough endoplasmic reticulum (Fig. 4, *C* and *D*).

These observations suggested that in thyroids of Cav-$1^{-/-}$ mice the iodination of Tg could take place inside the cells and not at the apical membrane-colloid interface. If this is the case, one would expect to find Duox and TPO in the cytoplasm and that they would be absent in the apical membrane. To test this hypothesis, we performed immunohistochemistry for these two enzymes in the thyroids of WT and Cav-$1^{-/-}$ mice. We found

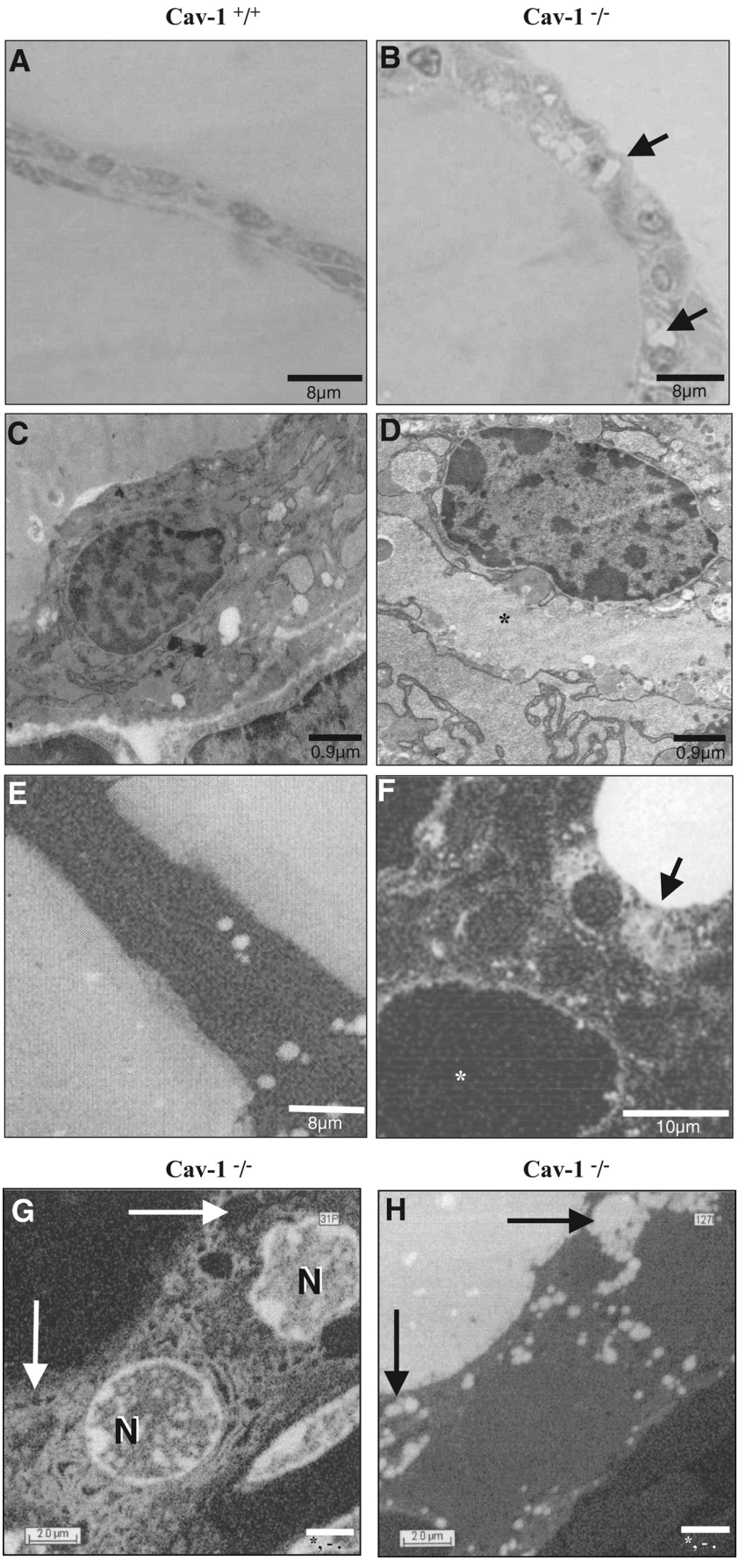

Fig. 3. *A* and *B*: semi-thin sections (0.5 μm thick) stained with toluidine blue. In Cav-$1^{-/-}$ mice (*B*), thyroid cells are taller than in WT, and they contain numerous large intracellular vesicles (arrows). *C* and *D*: TEM micrographs of WT (*C*) and Cav-$1^{-/-}$ (*D*) thyroids. Cav-$1^{-/-}$ thyrocytes show distension of the rough endoplasmic reticulum (*). *E* and *F*: ultrastructural distribution of ^{127}I by SIMS imaging. White areas correspond to iodine detection. *E*: in WT mice, ^{127}I is homogeneously distributed in the follicular lumina and in a few intracytoplasmic vesicles. *F*: in Cav-$1^{-/-}$ mice, some follicles (*) do not contain ^{127}I, which is instead detected in the cytoplasm and at the apical border. Accumulation of numerous cytoplasmic vesicles containig ^{127}I (arrow) is a hallmark of thyrocytes from Cav-$1^{-/-}$ mice. *G* and *H*: thyroid from Cav-$1^{-/-}$ mice. Ultrastructural distribution of ^{31}P (*G*) in the nuclei (N) and of ^{127}I (*H*). Intracytoplasmic ^{127}I localization (arrows) corresponds to dilated cisternae of endoplasmic reticulum (in black on *G*).

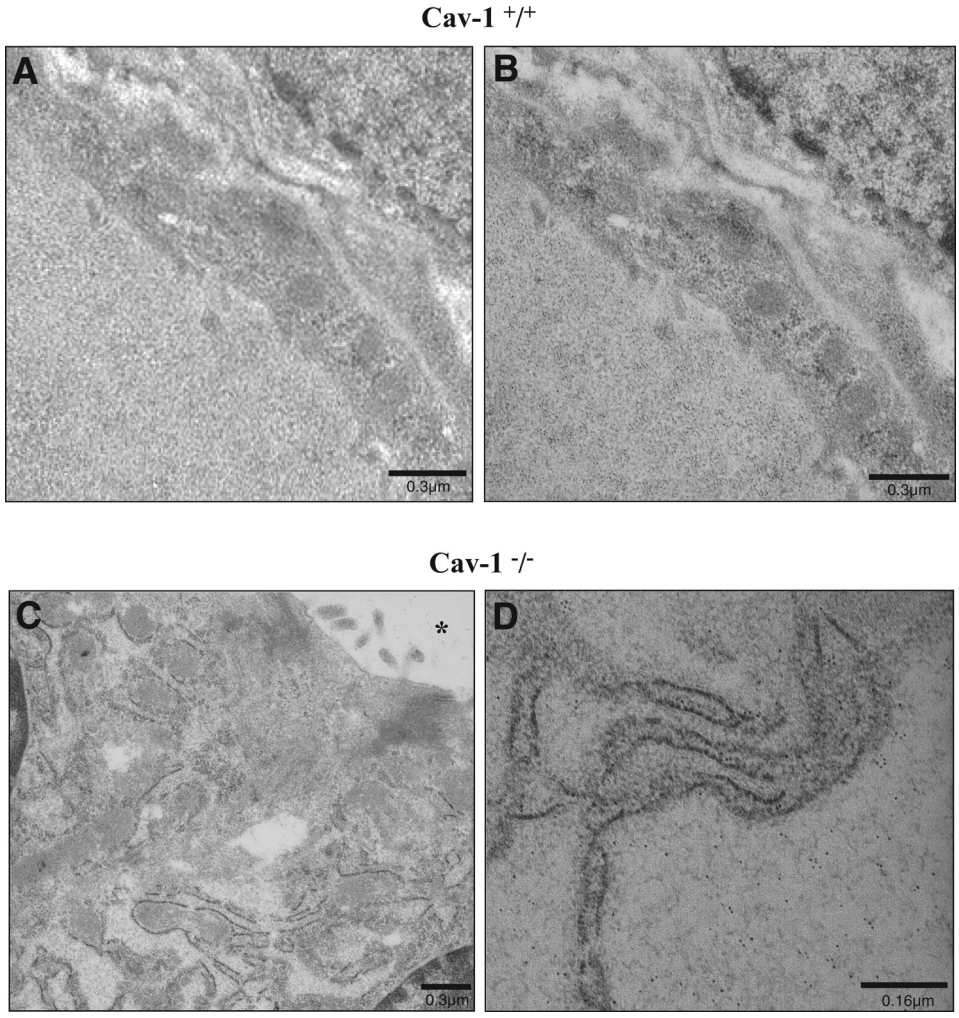

Fig. 4. Detection of Tg by immunogold electron microscopy. *A*: specificity control of immunolabeling by omission of the first antibody. *B*: in Cav-$1^{+/+}$ mice, Tg was detected as small gold particles in the colloid limited by flat epithelial cells. *C* and *D*: in Cav-$1^{-/-}$ mice, Tg was absent in some lumina (*) and detected in large dilatations of the rough endoplasmic reticulum.

that Duox is localized mainly in the cytoplasm of Cav-$1^{-/-}$ thyrocytes (Fig. 5*B*) and not at the apical membrane, as observed in the WT thyroids (Fig. 5*A*). Surprisingly, we also detected upregulation of Duox expression in Cav-$1^{-/-}$ thyroids. TPO could also be found in the cytoplasm of Cav-$1^{-/-}$ thyrocytes. Its expression was also increased in the abnormal follicles of Cav-$1^{-/-}$ thyroids (Fig. 5, *C* and *D*).

All together, these results indicate that the thyroids of Cav-$1^{-/-}$ mice present several functional abnormalities, namely, intracellular iodination and defective apical protein transport and luminal storage of Tg and iodide. To determine whether these phenotypes affect the overall efficiency of the iodination process, we measured the proportion of protein-bound $^{125}I^-$ (PBI) in the basal condition and upon stimulation by 10 mU/ml TSH. Although on average PBI in the basal condition was ~2.5-fold lower in Cav-$1^{-/-}$ thyroids than in the WT, the difference between the two groups was not statistically significant (Table 3). We also did not find any differences in the secretion of thyroid hormones in vitro between the Cav-$1^{-/-}$ and WT thyroids (Table 3). As a control, we verified that the in vitro $^{125}I^-$ uptake was also comparable between the two groups (Table 3). It must be emphasized that these studies investigate the follicles that have taken up and metabolized $^{125}I^-$. Open follicles (due to tissue section or to phenotype-related abnormalities) with no luminal $^{125}I^-$ accumulation do not contribute to these measurements.

In summary, we found that a proportion of Cav-$1^{-/-}$ thyrocytes display intracellular iodination and deficient transport of the thyroid hormone synthesis machinery to the apical membrane. However, these defects in altered follicles do not impair the overall iodide organification and the hormonal secretion that mainly reflect the intact follicles.

Lack of Cav-1 induces increased H_2O_2 generation, oxidative stress, cell damage, and apoptosis in thyrocytes. Normal thyroid cells generally exhibit very low cell turnover and apoptosis (20), but we had previously found (14) that Cav-$1^{-/-}$ thyrocytes have higher apoptotic rates than WT. In accord with this, TEM revealed the presence of several apoptotic nuclei and an accumulation of cell debris in the lumina of the most affected Cav-$1^{-/-}$ follicles (Fig. 6, *A* and *B*). Even more striking was the aberrant morphology of the apical membranes in the cells that constitute the most abnormal follicles (Fig. 6*A*). Taken together, these findings suggest that lack of Cav-1 causes cell damage in thyrocytes which ultimately leads to apoptosis.

The production of H_2O_2 by Duox is a key step in the hormonogenesis process, but it also represents a source of oxidative stress, even in a normal thyroid cell. The whole

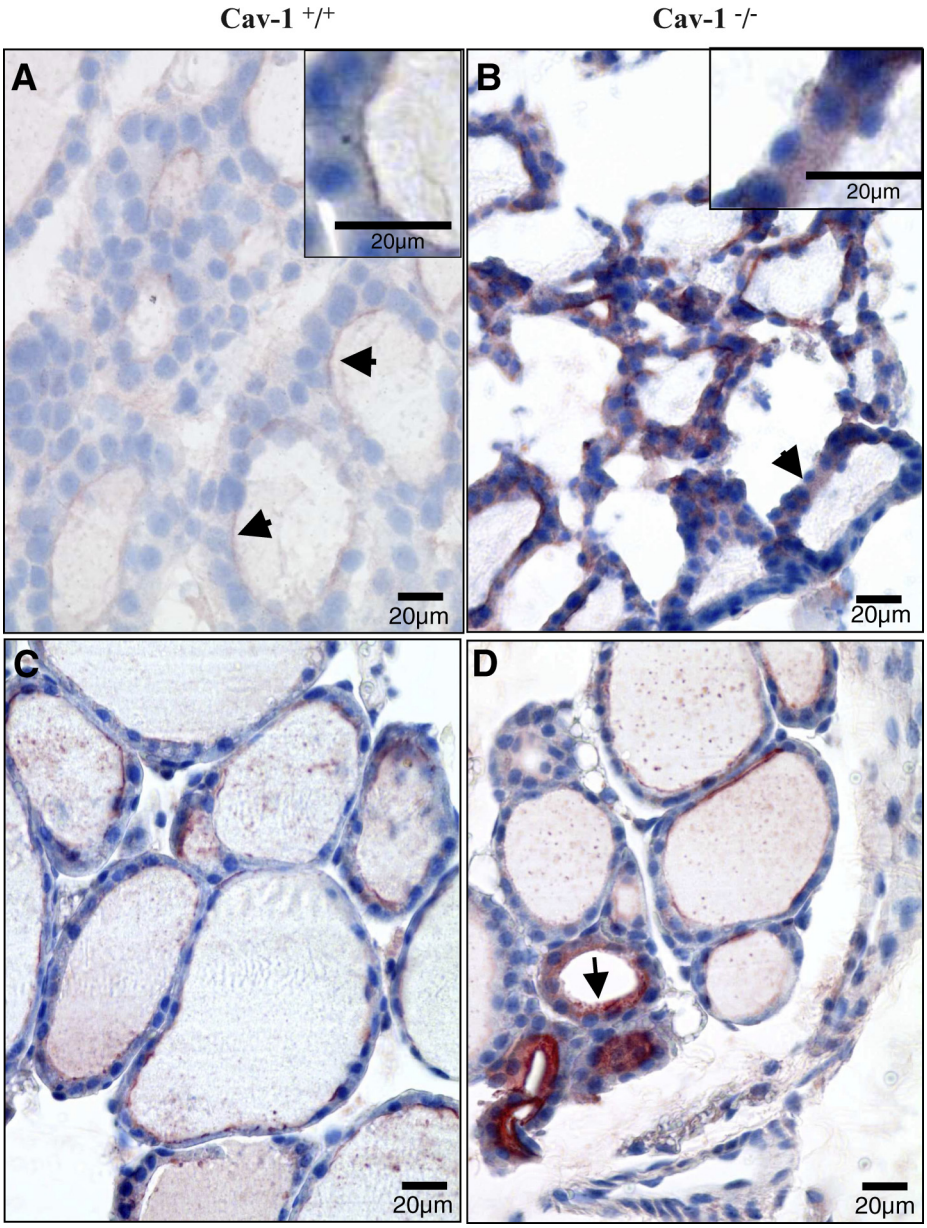

Fig. 5. Thyroid sections (5 μm thick) from Cav-$1^{+/+}$ (*A, C*) and Cav-$1^{-/-}$ (*B, D*) mice. *A* and *B*: immunodetection of dual oxidase (Duox) on frozen sections. In WT mice (*A*), Duox is detected at the apical pole (arrows, *inset*), whereas in Cav-$1^{-/-}$ mice (*B*), it is often localized in the cytoplasm (arrow, *inset*), and its expression is upregulated. *C and D*: immunodetection of thyroperoxidase (TPO) on paraffin sections. In Cav-$1^{-/-}$ mice (*D*), expression of TPO is also higher than in WT (*C*) and localized in the cytoplasm (arrow).

system in thyrocytes must be fine-tuned to produce strictly adequate and localized levels of H_2O_2, favoring hormone synthesis while avoiding damage due to excessive H_2O_2 amounts (54). In the thyroid of Cav-$1^{-/-}$ mice, Duox is mislocalized in the cytoplasm, and its expression level is increased. Therefore, it is possible that the cell damage and apoptosis detected in Cav-$1^{-/-}$ thyroids are caused by an excess of H_2O_2, i.e., H_2O_2 that is produced but not used to activate TPO, thus becoming available for (harmful) reaction with other cellular components. To test whether Cav-$1^{-/-}$ thyroids produce more H_2O_2, we measured the amount of H_2O_2 generated in vitro by Cav-$1^{-/-}$ and WT thyroids in basal condition and upon stimulation by 10 mU/ml TSH. We detected a highly significant increase in the H_2O_2 released by Cav-$1^{-/-}$ thyroids relative to their WT counterparts. However, the increase was statistically significant only in stimulated conditions. Considering that only about one-half of the follicles were affected, this increase is important. The increment in H_2O_2 production due to TSH stimulation was of the same order in the two groups (table 4). We must emphasize that the detected H_2O_2 only originates from the follicles opened by tissue section (54) and therefore merely reflects the activity of these follicles.

To assess whether the increase in the levels of H_2O_2 was translated into cellular oxidative stress and a potential cause of cell death, we performed immunohistochemistry to compare the relative amounts of three oxidative stress markers, HNE, peroxiredoxin 5 (PRDX5), and catalase, between the thyroids of WT and Cav-$1^{-/-}$ mice. HNE is a toxic aldehydic product resulting from the peroxidation of ω-6 unsaturated fatty acids present in cellular lipids (1). As such, its levels constitute a good indicator of the cellular damage due to oxidative stress. HNE was increased in Cav-$1^{-/-}$ thyrocytes compared with WT and even more in the cells of the "empty"

Table 3. *In vitro measurements of $^{125}I^-$ thyroidal uptake, PBI, and ^{125}I secretion as thyroid hormones*

	Basal	+TSH	*P*
$^{125}I^-$ uptake during 2-h incubation ($\times 10^3$ cpm per thyroid)			
WT	80±13	93±14	NS
Cav-1$^{-/-}$	112±23	111±27	NS
P	NS	NS	
PBI (% of total thyroidal ^{125}I) 2 h incubation			
WT	13.1±4.4	20.5±3.4	< 0.05
Cav-1$^{-/-}$	5.0±1.1	23.2±5.9	< 0.01
P	NS	NS	
^{125}I secretion as thyroid hormones during 3-h incubation (%butanol-extractable ^{125}I in the incubation medium)			
WT	1.5±0.3	12.9±1.5	< 0.001
Cav-1$^{-/-}$	1.3±0.1	10.9±1.4	< 0.001
P	NS	NS	

Values represent means ± SE of 6 mice per group. TSH concentrations used were 10 mU/ml for $^{125}I^-$ thyroidal uptake, 10 mU/ml for protein-bound ^{125}I (PBI), and 5 mU/ml for ^{125}I secretion. Analysis per paired sample of each series.

Table 4. *H_2O_2 levels (ng /ml) generated in vitro during 3-h incubation*

	Basal	TSH, 10 mU/ml	*P*
WT	10.6±0.7	15.4±1.7	NS
Cav-1$^{-/-}$	15.7±2.1	23.5±1.6	< 0.02
P	NS	< 0.02	

Values represent mean ± SE of 4 mice per group (paired comparisons in 4 series). When all WT samples (basal or with TSH) are compared to Cav-1$^{-/-}$ in a series of 8, the difference is significant with $P < 0.005$. n.s.: no statistically significant difference.

follicles (Fig. 7, *A* and *B*). PRDX5 is a detoxifying thioredoxin-dependent enzyme used by mammalian cells to reduce peroxides and peroxinitrites. It is localized in the cytosol, mitochondria, and peroxisomes (33). PRDX5 is expressed in the normal human thyroid, and its levels directly correlate with the functional status of thyrocytes (26). We observed that PRDX5 expression was upregulated in the abnormal follicles of Cav-1$^{-/-}$ mice, which suggested an increased oxidative stress in the absence of Cav-1 and a higher cell protection (Fig. 7, *C* and *D*). Finally, catalase, detected in the cytoplasm of thyroid cells from WT mice (Fig. 7*E*), was upregulated in follicles from Cav-1$^{-/-}$ mice (Fig. 7*F*).

We therefore conclude that Cav-1 deficiency in thyroid follicular cells leads to an excess of intracellular H_2O_2, which increases the oxidative stress and could be, at least in part, responsible for the observed cell damage and apoptosis (14). Of course, other mechanisms could also contribute to these effects. All the described abnormalities were detected within the same follicles, as shown on serial sections: absence of PAS staining and of Tg-I in the lumen, mislocalization and overexpression of Duox and TPO, and increased levels of PRDX5 and HNE (Fig. 8).

Cav-1$^{-/-}$ mice have normal levels of free T_4 and TSH. Given the detected cellular defects, we wanted to investigate the possibility of a mild hypothyroidal phenotype. We measured the levels of free (active) T_3 and T_4 in the serum of 10-mo-old WT and Cav-1$^{-/-}$ mice. In Cav-1$^{-/-}$ mice, we found a mild, yet statistically significant, decrease in the levels of free T_3, but the levels of free T_4 were comparable to those found in the sera of WT mice (Table 5). Serum TSH levels are the most sensitive indicator of thyroid function (22). We measured the serum TSH activity in WT and Cav-1$^{-/-}$ mice by use of a bioassay but did not find differences between the two groups (Table 5). However, the variation between the individual values is large, and this could mask differences. Serum TSH level determined by the TSH bioassay were validated by direct measurement of TSH by RIA (data not shown). Therefore, there is no evidence of hypothyroidism, and the malfunctioning of the empty follicles is compensated by the activity of the less affected follicles.

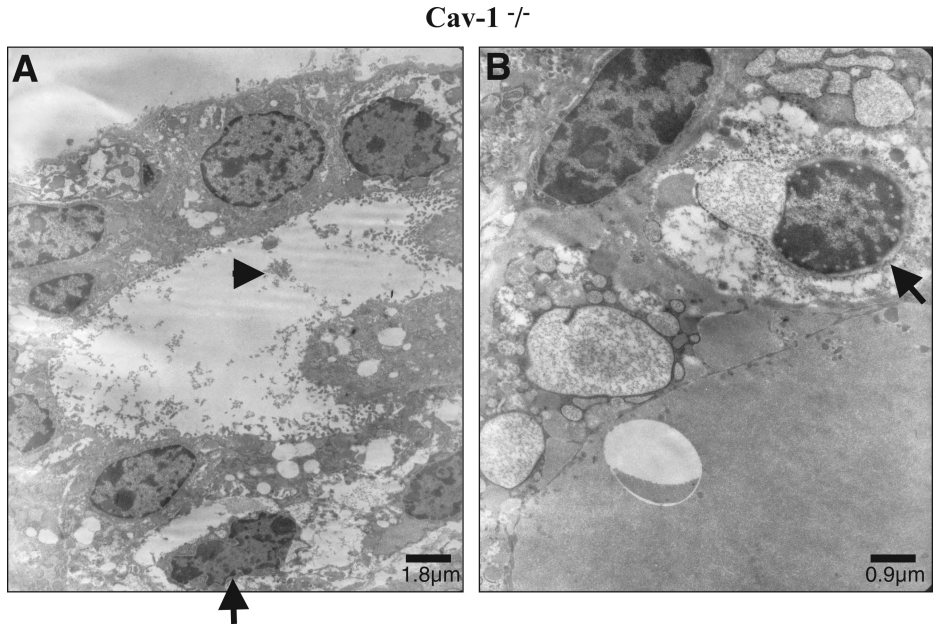

Fig. 6. TEM micrographs of Cav-1$^{-/-}$ thyroids. *A*: follicular lumen contains cell debris and shed membranes (short arrow). Apoptotic cells (long arrows) are recognized by their pycnotic nuclei (*A* and *B*) and large dilatations of the endoplasmic reticulum.

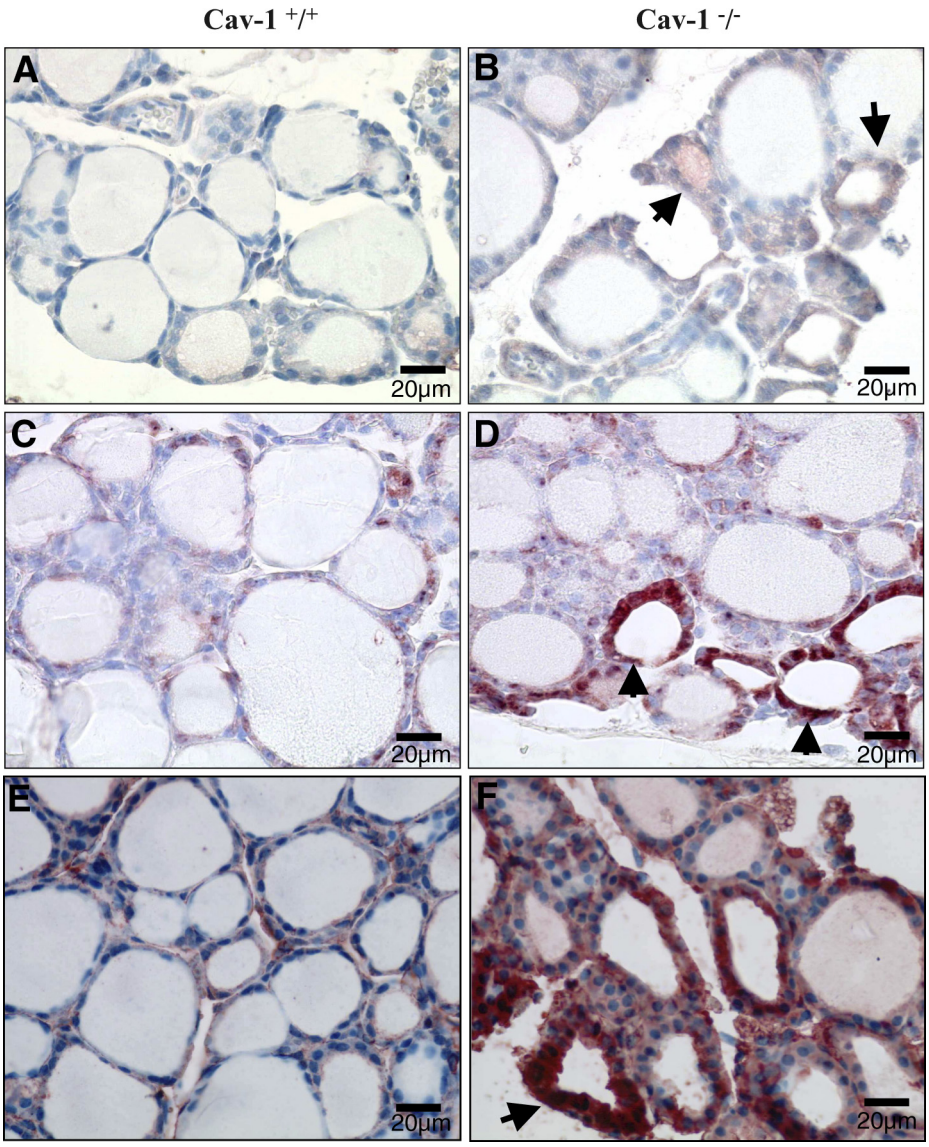

Fig. 7. Thyroid sections (5 μm thick) from Cav-1$^{+/+}$ (*A, C, E*) and Cav-1$^{-/-}$ (*B, D, F*) mice. *A* and *B*: immunodetection of HNE. 4-Hydroxynonenal (HNE) production is increased in thyroid of Cav-1$^{-/-}$ mice (*B*), particularly in the more abnormal follicles (arrows). *C* and *D*: immunodetection of peroxiredoxin 5 (PRDX5). PRDX5 is highly expressed in "empty" follicles (arrows) observed in Cav-1$^{-/-}$ mice (*D*). *E* and *F*: immunodetection of catalase. In Cav-1$^{+/+}$ mice (*E*), catalase is detected in the cytoplasm. Its cytoplasmic expression is strongly increased in thyroids from Cav-1$^{-/-}$ mice (*F*).

DISCUSSION

In the present work, we performed a comprehensive analysis of the thyroidal phenotype of Cav-1$^{-/-}$ mice to determine the role that Cav-1 plays at the apical region of thyrocytes (13) and how lack of this protein in thyrocytes might lead to apoptosis (14). Our investigation leads to the main conclusion that, primarily, Cav-1 in thyroid follicular cells is involved in the proper apical sorting/transport of at least some components (Tg, Duox, TPO) of the hormone synthesis machinery.

The requirement of Cav-1 in the sorting of membrane-resident proteins was also reported in the case of the angiotensin II receptor (60), the insulin receptor (11), the stretch-activated channel short transient receptor potential channel-1 (TRPC1) (8), and the fatty acid translocase FAT/CD36 (49).

There are several reasons to think that the other phenotypes, i.e., characteristics found in the deficient thyroid are, at least to some extent, secondary effects of the mislocalization of the involved proteins and/or the "end state" resulting from compensatory mechanisms that were developed. First, we have found absence of luminal PAS staining, mislocalization, and overexpression of Duox and TPO and increased amounts of PRDX5 and HNE within the same Cav-1$^{-/-}$ thyroid follicles. Second, the accumulation of large vesicles and the intracellular iodination may be direct consequences of the retention and activity in the cytosol of the unsorted Tg, TPO, and Duox. Third, the square shape of thyrocytes and the distension of the rough endoplasmic reticulum could result from a cell response to the deficient thyroid hormone synthesis (e.g., increased expression of Duox, TPO, and PRDX5). Fourth, because Duox is mislocalized in the cytoplasm and its expression levels are increased, one might expect that the high concentration of H_2O_2 may be a consequence of both the high Duox expression and the lack of tonic inhibition of Duox activity by Cav-1. The high production of H_2O_2 detected in Cav-1$^{-/-}$ thyroids is in agreement with a report that intracellular Duox could in some circumstances have the ability to generate H_2O_2 (4). In favor of the hypothesis of direct inhibition of Duox by Cav-1, there are three amino acid sequences (1203YVFASHHFRRRFRGF1217, 1295FEYKSGQW1302, and 1490FGRPPFEPF1498), conserved between Duox1 and Duox2, that might constitute consensus

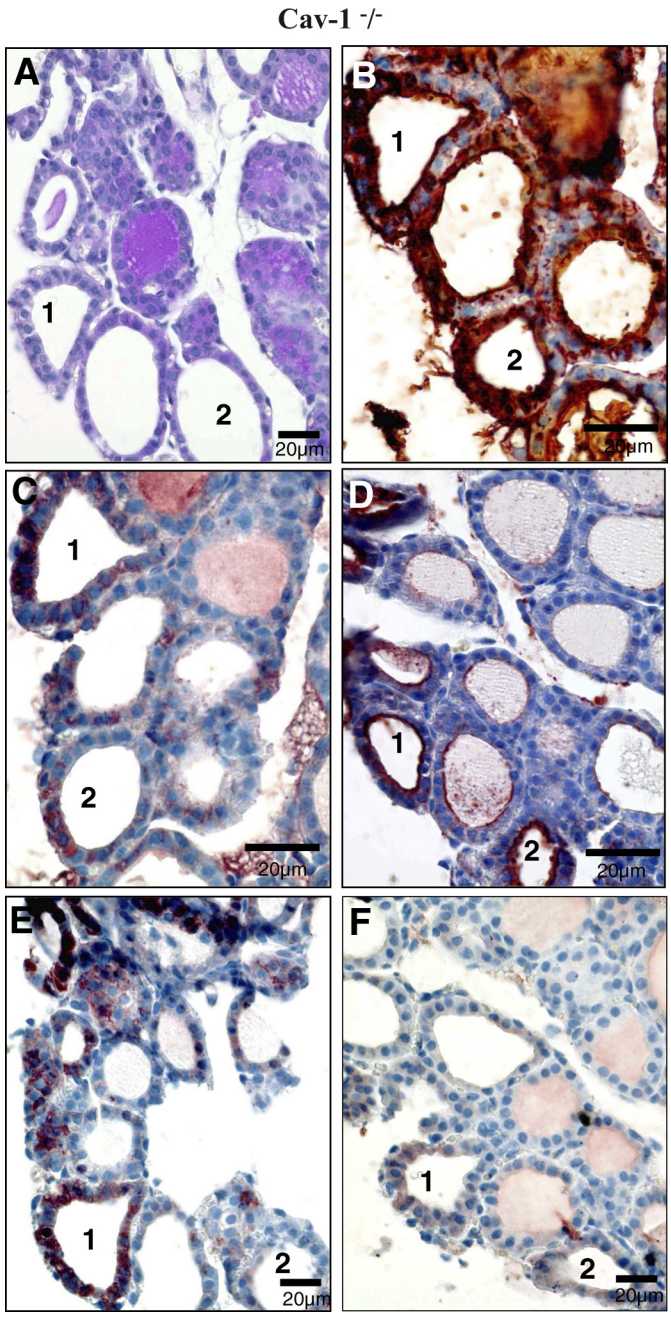

Fig. 8. Serial sections (5 μm thick) from thyroid of a Cav-$1^{-/-}$ mouse. Follicles 1 and 2 lack PAS staining (*A*) and Tg-I staining (*B*), Tg-I being accumulated in the cytoplasm and at the apical border. The same follicles display high expression of Duox (*C*) and TPO (*D*) in the cytoplasm. They also show increased expression of PRDX5 (*E*) and HNE production (*F*).

binding sites to the so-called Cav-1 scaffolding domain (15). All these sequences are in the cytoplasmic region, two localized near the binding sites of FAD and of NADPH and a third one corresponding to the entire intracellular loop between domains V and VI (for a representation of the amino acid sequence and the presumed membrane topology of Duox, see Refs. 16). As these sites are in the cytoplasmic region of Duox, they are good candidates for an interaction with the scaffolding domain of Cav-1, which is also localized in the cytoplasmic region of the protein. A homolog of Duox expressed in vascular smooth muscle cells, Nox1, is localized in Cav-1-enriched membranes (30). In these cells, knockdown of Cav-1 results in an inhibition of H_2O_2 release as a consequence of the failure of Rac1 (a positive regulator of Nox1) to translocate to the membrane and to activate in the absence of Cav-1 (62). However, in thyroid, the regulation of Duox activity does not involve Rac1 activation (21). This diversity in the regulation of the various NADPH oxidases may help to explain the opposite effects of Cav-1 depletion on H_2O_2 levels between these two cell types. Fifth, the simplest explanation for the detected increase of oxidative stress in Cav-$1^{-/-}$ thyrocytes is the availability of H_2O_2. Sixth, the observed cell and tissue damage (present work) and apoptosis [present and previous work (14)] are very likely a direct consequence of the oxidative stress to which Cav-$1^{-/-}$ thyroid cells are exposed. This is demonstrated by the increase of H_2O_2 and HNE levels. HNE, by modiying proteins involved in cell homeostasis and biological signaling, is known to play a role in the pathogenesis of several diseases (43). However, the thyroid cells develop protective systems against the increased H_2O_2 production, as shown by the upregulation of PRDX5 and catalase. It is interesting in this regard that Cav-1 depletion is not compensated for by upregulation of Cav-2 expression, as the latter was absent in Cav-1 mice, in agreement with the fact that Cav-$1^{-/-}$ drives the expression of Cav-2 (37). Finally, the increase in the apoptotic rate in Cav-$1^{-/-}$ thyrocytes is proportionally compensated for by the cell proliferation index (14), thus preventing a decrease in the overall thyroid gland size and function. Because Cav-1 is a multifunctional protein, this balance between proliferation and apoptosis in Cav-$1^{-/-}$ thyroid cells raises the question: is the increased proliferation rate of Cav-$1^{-/-}$ thyroid cells merely a compensatory response to the cell death or is it a direct consequence of the absence of Cav-1? We favor the latter hypothesis, because when we blocked the production of thyroid hormones through a low-iodine chow and $NaClO_4$ in the drinking water, the induced goiter was more developed in Cav-$1^{-/-}$ mice (Fig. 9). Moreover, our previous work (14) demonstrated the reciprocal negative regulation between TSH/cAMP-mediated proliferation and Cav-1 expression. Such compensations and the fact that one-half of the thyroid follicles do not show an overt phenotype could explain the normal overall iodide organification, secretion of thyroid hormones, and free T_4 and TSH levels. However, the wide variation in TSH bioactivity could mask a small but significant TSH increase in Cav-$1^{-/-}$ mice. Of course, an indirect effect on thyrocytes of Cav-1 lack in other cell types might contribute to the thyroid phenotype and would only be excluded by thyrocyte-specific knockouts.

Table 5. *Serum levels of free thyroid hormones and TSH bioassay*

	WT	Cav-$1^{-/-}$	
Thyroid hormones	(n = 5)	(n = 6)	
fT_3, pg/ml	3.2±0.2	2.3±0.1	$P < 0.05$
fT_4, ng/dl	2.4±0.1	2.0±0	NS
TSH bioactivity	(n = 13)	(n = 13)	
cAMP, pmol/tube	1.5±0.3	1.5±0.3	

Results are expressed as means ± SD. fT_3, free triiodothyronine; fT_4, free thyroxine.

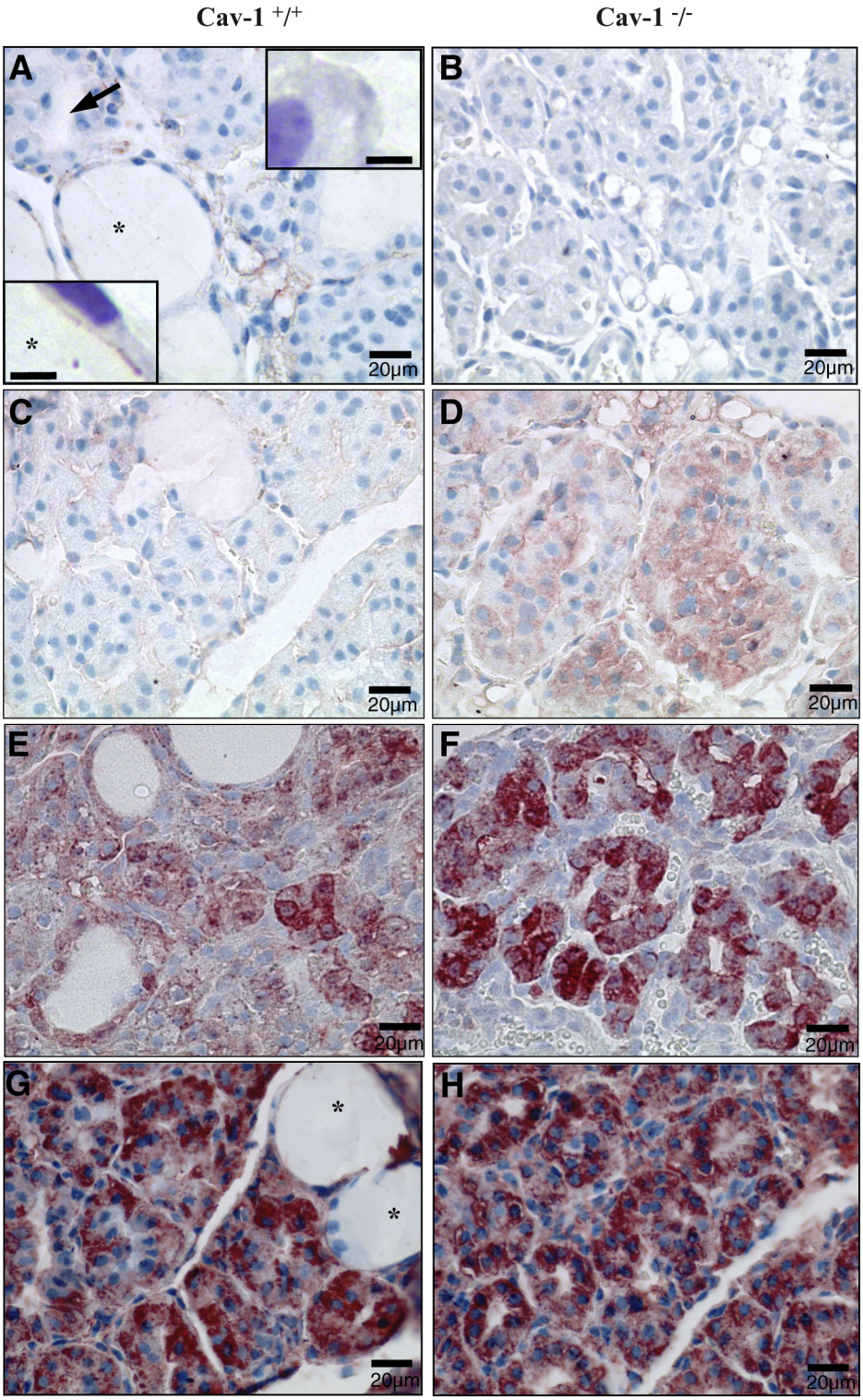

Fig. 9. Thyroid sections (5 μm thick) from goitrous Cav-$1^{+/+}$ (*A, C, E, G*) and Cav-$1^{-/-}$ (*B, D, F, H*) mice. *A* and *B*: immunodetection of Cav-1. In Cav-$1^{+/+}$ mice (*A*), some follicles are hyperplastic (arrows), while others keep a resting aspect with a flat epithelial layer (*). In these resting follicles (*), Cav-1 was detected at the apical pole (*inset*; bar, 5 μm), whereas in hyperplastic follicles, Cav-1 was not detected (*inset*; bar, 5 μm). In Cav-$1^{-/-}$ mice (*B*), the response to the goiterogenic stimulus is well marked in all follicles having a hyperplastic aspect. Cav-1 is not detected. *C* and *D*: immunodetection of HNE. HNE expression is more intense in Cav-$1^{-/-}$ mice (*D*) than in WT mice (*C*). *E* and *F*: immunodetection of PRDX5. PRDX5 expression is increased by goiterogenic stimulus but is higher in Cav-$1^{-/-}$ mice (*F*) than in WT (*E*). *G* and *H*: immunodetection of catalase. In goitrous WT mice (*G*), catalase expression is very high in hyperplastic follicles compared with resting follicles (*). It is intense in all follicular cells of goitrous Cav-$1^{-/-}$ mice (*H*).

Our results are consistent with the mild phenotype of Cav-$1^{-/-}$ mice and with the concept that some of the observed features of these mice result from the balance between the defects and compensatory mechanisms (32). Such mechanisms have been described in several cell types, even in those in which the expression of Cav-1 is the most abundant. For instance, in white adipose tissue, lack of Cav-1 leads to tissue abnormalities and downregulation of insulin receptor protein expression, but the serum levels of glucose and insulin remain entirely normal (46, 11). Some authors have suggested that it is the existence of such compensatory processes that explains the viability of Cav-$1^{-/-}$ mice (19, 34). As reported for other tissue types (46, 12, 35), a more prominent thyroid phenotype was observed when the thyrocytes were challenged by the artificially increased TSH levels referred to above.

The observed decrease of free T_3 levels in Cav-$1^{-/-}$ mice may be related to phenotypes described (and/or still unknown) in other cell types. Neurological abnormalities were described in Cav-$1^{-/-}$ mice: reduced brain size and associated motor and behavioral problems. These features could be appreciated only in aged (>1-yr-old) animals (55) and are thus unlikely related to the thyroid gland phenotype but might reflect, at least in part, a lower T_4-to-T_3 deiodination. Some of the reported phenotypes of Cav-$1^{-/-}$ mice resemble the phenotype of mice lacking the thyroid hormone receptor $\alpha 1$, body temperature $\approx$0.5°C lower than normal and mild hypothyroidism, whereas their overall behavior and reproduction are normal (19, 12, 59).

Several studies have suggested the existence of sphingolipid-cholesterol-enriched domains in the apical membrane of follicular cells. These studies preceded the discovery of Cav-1 (51, 33) and the lipid "rafts" hypothesis (53). They reported the accumulation of cholesterol at the apical membrane of the cell in mouse (23) and in rat and porcine (6) thyroids. It was also demonstrated that fractions of bovine thyroid enriched in apical membranes have low fluidity (18), which is a hallmark of sphingolipid-cholesterol-enriched membrane domains. Together with our findings that Cav-1 is localized in the apical region of thyrocytes, this literature supports the existence of caveolae in the apical membrane of thyrocytes. Moreover, in the Fisher rat thyroid cell line, the formation of caveolae is obtained after Cav-1 transfection (36), and we have shown the existence of caveolae in thyroid cells from control mice. However, it is now recognized that Cav-1 can also regulate cell mechanisms outside of caveolae and that the study of Cav-$1^{-/-}$ mice does not distinguish between the actions of caveolins within or outside of caveolae in cells containing caveolae (29). Therefore, even if such organelles exist in the apical membrane of thyroid cells, it is still possible that the role played by Cav-1 in that membrane is unrelated to the caveolar pool of Cav-1.

As discussed, Cav-$1^{-/-}$ thyroids do not show evidence of tumor initiation, but Cav-1 expression is downregulated in ~80% of human thyroid follicular carcinomas (2, 3) and in thyroid autonomous adenomas (58). Given the oxidative stress present in Cav-$1^{-/-}$ thyroid cells, we predict that the downregulation of Cav-1 expression would further disrupt the tissue homeostasis in these differentiated tumor types. PRDX5 expression is indeed upregulated in various thyroid pathologies (26). It would be interesting to compare the oxidative stress between differentiated thyroid tumor samples that display, or not, Cav-1 downregulation in order to assess whether Cav-1 expression indeed negatively correlates with increased oxidative stress. It would also be interesting to analyze the microvascular bed surrounding follicles with a high or low expression of Cav-1. Indeed, it determines, by the production of VEGF and NO, the functional status of the follicles, known to be greatly heterogenous in animal and human thyroids (24, 25).

ACKNOWLEDGMENTS

We are thankful to Dr. F. Miot (Institut de Recherche Interdisciplinaire, Brussels, Belgium), Dr. B. Knoops (Université Catholique de Louvain, Belgium) and Dr. J. de Vijlder (University of Amsterdam, The Netherlands), who provided the antibodies for Duox, PRDX5, and Tg-I, respectively, and Dr. C. Gervy (Hôpital Erasme, Brussels, Belgium), for help with measurements of free T_3 and free T_4. We are also very grateful to Dr. S. Refetoff (University of Chicago) for kindly performing the TSH RIA for us. We thank Prof. J. Rahier, A. Lefevre, and C. de Ville de Goyet for performing the TEM analysis.

GRANTS

This work was supported by Fonds National pour la Recherche Scientifique, Fonds de la Recherche Scientifique Médicale, Ministère de la Politique Scientifique (PAI), Fondation Van Buuren, Fondation Rose et Jean Hoguet, and Fundação para a Ciência e a Tecnologia (Portugal, fellowship to M. J. Costa).

REFERENCES

1. **Alary J, Gueraud F, Cravedi JP.** Fate of 4-hydroxynonenal in vivo: disposition and metabolic pathways. *Mol Aspects Med* 24: 177–187, 2003.
2. **Aldred MA, Ginn-Pease ME, Morrison CD, Popkie AP, Gimm O, Hoang-Vu C, Krause U, Dralle H, Jhiang SM, Plass C, Eng C.** Caveolin-1 and caveolin-2, together with three bone morphogenetic protein-related genes, may encode novel tumor suppressors down-regulated in sporadic follicular thyroid carcinogenesis. *Cancer Res* 63: 2864–2871, 2003.
3. **Aldred MA, Huang Y, Liyanarachchi S, Pellegata NS, Gimm O, Jhiang S, Davuluri RV, de la Chapelle A, Eng C.** Papillary and follicular thyroid carcinomas show distinctly different microarray expression profiles and can be distinguished by a minimum of five genes. *J Clin Oncol* 22: 3531–3539, 2004.
4. **Ameziane-El-Hassani R, Morand S, Boucher JL, Frapart YM, Apostolou D, Agnandji D, Gnidehou S, Ohayon R, Noel-Hudson MS, Francon J, Lalaoui K, Virion A, and Dupuy C.** Dual oxidase-2 has an intrinsic Ca2+-dependent H2O2-generating activity. *J Biol Chem* 280: 30046–30054, 2005.
5. **Audinot JN, Senou M, Migeon HN, Many MC.** Visualisation of thyroid hormone synthesis by ion imaging. *Applied Surface Sci* 130: 1–8, 2008.
6. **Barriere H, Chailley B, Chambard M, Selzner JP, Mauchamp J, Gabrion J.** Cholesterol-rich microdomains in rat and porcine thyroid membranes involved in TSH-induced endocytotic processes. *Acta Anat (Basel)* 132: 205–215, 1988.
7. **Benard B, Brault J.** [Production of peroxide in the thyroid]. *Union Med Can* 100: 701–705, 1971.
8. **Brazer SC, Singh BB, Liu X, Swaim W, Ambudkar IS.** Caveolin-1 contributes to assembly of store-operated Ca2+ influx channels by regulating plasma membrane localization of TRPC1. *J Biol Chem* 278: 27208–27215, 2003.
9. **Brooker G, Harper JF, Terasaki WL, Moylan RD.** Radioimmunoassay of cyclic AMP and cyclic GMP. *Adv Cyclic Nucleotide Res* 10: 1–33, 1979.
10. **Castaing R, Slodzian G.** Microanalyse par emission ionique secondaire. *Journal* of Microscopy 1, 395–410, 1962.
11. **Cohen AW, Razani B, Wang XB, Combs TP, Williams TM, Scherer PE, Lisanti MP.** Caveolin-1-deficient mice show insulin resistance and defective insulin receptor protein expression in adipose tissue. *Am J Physiol Cell Physiol* 285, C222–C235, 2003.
12. **Cohen AW, Schubert W, Brasaemle DL, Scherer PE, Lisanti MP.** Caveolin-1expression is essential for proper nonshivering thermogenesis in brown adipose tissue. *Diabetes* 54: 679–686, 2005.
13. **Costa MJ, Song Y, Macours P, Massart C, Many MC, Costagliola S, Dumont JE, Van Sande J, Vanvooren V.** Sphingolipid-cholesterol domains (lipid rafts) in normal human and dog thyroid follicular cells are not involved in thyrotropin receptor signaling. *Endocrinology* 145: 1464–1472, 2004.
14. **Costa MJ, Senou M, Van Rode F, Ruf J, Capello M, Dequanter D, Lothaire P, Dessy C, Dumont JE, Many MC, Van Sande J.** Reciprocal negative regulation between thyrotropin/3′,5′-cyclic adenosine monophosphate-mediated proliferation and caveolin-1 expression in human and murine thyrocytes. *Mol Endocrinol* 21: 921–932, 2007.
15. **Couet J, Li S, Okamoto T, Ikezu T, Lisanti MP.** Identification of peptide and protein ligands for the caveolin-scaffolding domain. Implications for the interaction of caveolin with caveolae-associated proteins. *J Biol Chem* 272: 6525–6533, 1997.
16. **De Deken X, Wang D, Many MC, Costagliola S, Libert F, Vassart G, Dumont JE, Miot F.** Cloning of two human thyroid cDNAs encoding new members of the NADPH oxidase family. *J Biol Chem* 275: 23227–23233, 2000.
17. **Den Hartog MT, De Boer M, Veenboer GJ, de Vijlder JJ.** Generation and characterization of monoclonal antibodies directed against noniodinated and iodinated thyroglobulin, among which are antibodies against hormonogenic sites. *Endocrinology* 127: 3160–3165, 1990.
18. **Depauw H, de Wolf M, van Dessel G, Hilderson HJ, Lagrou A, Dierick W.** Fluidity characteristics of bovine thyroid plasma membranes. *Biochim Biophys Acta* 814: 57–67, 1985.

19. **Drab M, Verkade P, Elger M, Kasper M, Lohn M, Lauterbach B, Menne J, Lindschau C, Mende F, Luft FC, Schedl A, Haller H, Kurzchalia TV.** Loss of caveolae, vascular dysfunction, and pulmonary defects in caveolin-1 gene-disrupted mice. *Science* 293: 2449–2452, 2001.
20. **Dremier S, Golstein J, Mosselmans R, Dumont JE, Galand P, Robaye B.** Apoptosis in dog thyroid cells. *Biochem Biophys Res Commun* 200: 52–58, 1994.
21. **Fortemaison N, Miot F, Dumont JE, Dremier S.** Regulation of H2O2 generation in thyroid cells does not involve Rac1 activation. *Eur J Endocrinol* 152: 127–133, 2005.
22. **Franklyn JA.** Subclinical thyroid disorders—consequences and implications for treatment. *Ann Endocrinol (Paris)* 68: 229–230, 2007.
23. **Fujita H, Ishimura K, Matsuda H.** Freeze-fracture images on filipin-sterol complexes in the thyroid follicle epithelial cell of mice with special regard to absence of cholesterol at the site of micropinocytosis. *Histochemistry* 73: 57–63, 1981.
24. **Gerard AC, Xhenseval V, Colin IM, Many MC, Denef JF.** Evidence for co-ordinated changes between vascular endothelial growth factor and nitric oxide synthase III immunoreactivity, the functional status of the thyroid follicles, and the microvascular bed during chronic stimulation by low iodine and propylthiouracyl in old mice. *Eur J Endocrinol* 142: 651–660, 2000.
25. **Gerard AC, Many MC, Daumerie C, Costagliola S, Miot F, Devijlder JJ, Colin IM, Denef JF.** Structural changes in angiofollicular units between active and hypofunctioning follicles align with differences in the epithelial expression of newly discovered proteins involved in iodine transport and organification. *J Clin Endocrinol* 87: 1294–1299, 2002.
26. **Gerard AC, Many MC, Daumerie C, Knoops B, Colin IM.** Peroxiredoxin 5 expression in the human thyroid gland. *Thyroid* 15: 205–209, 2005.
27. **Gerard AC, Poncin S, Caetano B, Sonveaux P, Audinot JN, Feron O, Colin IM, Soncin F.** Iodine deficiency induces a thyroid stimulating hormone-independent early phase of microvascular reshaping in thyroid. *Am J Pathol* 172: 748–60, 2008.
28. **Guerquin-Kern JL, Hillion F, Madelmont JC, Labarre P, Papon J, Croisy A.** Ultra-structural cell distribution of the melanoma marker iodobenzamide: improved potentiality of SIMS imaging in life sciences. *Biomed Eng Online* 3: 1–7, 2004.
29. **Head BP, Insel PA.** Do caveolins regulate cells by actions outside of caveolae? *Trends Cell Biol* 17: 51–57, 2007.
30. **Hilenski LL, Clempus RE, Quinn MT, Lambeth JD, Griendling KK.** Distinct subcellular localizations of Nox1 and Nox4 in vascular smooth muscle cells. *Arterioscler Thromb Vasc Biol* 24: 677–683, 2004.
31. **Hnasko R, Lisanti MP.** The biology of caveolae: lessons from caveolin knockout mice and implications for human disease. *Mol Interv* 3: 445–464, 2003.
32. **Insel PA, Patel HH.** Do studies in caveolin knockouts teach us about physiology and pharmacology or instead, the ways mice compensate for 'loss protein'? *Br J Pharmacol* 150: 251–254, 2007.
33. **Kurzchalia TV, Dupree P, Parton RG, Kellner R, Virta H, Lehnert M, Simons K.** VIP21, a 21-kD membrane protein is an integral component of trans-Golgi-network-derived transport vesicles. *J Cell Biol* 118: 1003–1014, 1992.
34. **Le Lay S, Kurzchalia TV.** Getting rid of caveolins: phenotypes of caveolin-deficient animals. *Biochim Biophys Acta* 1746: 322–333, 2005.
35. **Li J, Scherl A, Medina F, Frank PG, Kitsis RN, Tanowitz HB, Sotgia F, Lisanti MP.** Impaired phagocytosis in caveolin-1 deficient macrophages. *Cell Cycle* 4: 1599–1607, 2005.
36. **Lipardi C, Mora R, Colmer V, Paladino S, Nitsch L, Rodriguez-Boulan E, Zurzolo C.** Caveolin transfection results in caveolae formation but not apical sorting of glycosylphosphatidylinositol (GPI)-anchored proteins in epithelial cells. *J Cell Biol* 140: 617–626j, 1998.
37. **Mora R, Bonihla VL, Marmostein A, Scherer PE, Brown D, Lisanti MP, Rodriguez-Boulan E.** Caveolin-2 localizes to the golgi complex but redistributes to plasma membrane, caveolea, and rafts when coexpressed with caveolin-1. *J Biol Chem* 274: 25708–25717, 1999.
38. **Palade GE.** Fine structure of blood capillaries. *J Appl Physiol* 24: 1424–1436, 1953.
39. **Park DS, Cohen AW, Frank PG, Razani B, Lee H, Williams TM, Chandra M, Shirani J, De Souza AP, Tang B, Jelicks LA, Factor SM, Weiss LM, Tanowitz HB, Lisanti MP.** Caveolin-1 null (−/−) mice show dramatic reductions in life span. *Biochemistry* 42: 15124–15131, 2003.
40. **Parton RG, Hanzal-Bayer M, Hancock JF.** Biogenesis of caveolae: a structural model for caveolin-induced domain formation. *J Cell Sci* 119: 787–796, 2006.
41. **Perret J, Ludgate M, Libert F, Gerard C, Dumont JE, Vassart G, Parmentier M.** Stable expression of the human TSH receptor in CHO cells and characterization of differentially expressing clones. *Biochem Biophys Res Commun* 171: 1044–1050, 1990.
42. **Peteranderl R, Lechene C.** Measure of carbon and nitrogen stable isotope ratios in cultured cells. *J Am Soc Mass Spectrom* 15: 478–485, 2004.
43. **Petersen DR, Doorn JA.** Reactions of 4-hydroxynonenal with proteins and cellular targets. *Free Radic Biol Med* 37: 937–945, 2004.
44. **Pohlenz J, Maqueem A, Cua K, Weiss RE, Van Sande J, Reffetoff S.** Improved radioimmunoassay for measurement of mouse thyrothropin in serum: strain difference in thyrotropin concentration and thyrotroph sensitivity to thyroid hormone. *Thyroid* 9: 1265–1271, 1999.
45. **Razani B, Combs TP, Wang XB, Frank PG, Park DS, Russell RG, Li M, Tang B, Jelicks LA, Scherer PE, Lisanti MP.** Caveolin-1-deficient mice are lean, resistant to diet-induced obesity, and show hypertriglyceridemia with adipocyte abnormalities. *J Biol Chem* 277: 8635–8647, 2002.
46. **Razani B, Engelman JA, Wang XB, Schubert W, Zhang XL, Marks CB, Macaluso F, Russell RG, Li M, Pestell RG, Di Vizio D, Hou H Jr, Kneitz B, Lagaud G, Christ GJ, Edelmann W, Lisanti MP.** Caveolin-1 null mice are viable but show evidence of hyperproliferative and vascular abnormalities. *J Biol Chem* 276: 38121–38138, 2001.
47. **Razani B, Woodman SE, Lisanti MP.** Caveolae: from cell biology to animal physiology. *Pharmacol Rev* 54: 431–467, 2002.
48. **Rhee SG, Chae HZ, Kim K.** Peroxiredoxins: a historical overview and speculative preview of novel mechanisms and emerging concepts in cell signaling. *Free Radic Biol Med* 38: 1543–1552, 2005.
49. **Ring A, Le Lay S, Pohl J, Verkade P, Stremmel W.** Caveolin-1 is required for fatty acid translocase (FAT/CD36) localization and function at the plasma membrane of mouse embryonic fibroblasts. *Biochim Biophys Acta* 1761: 416–423, 2006.
50. **Rodesch F, Neve P, Willems C, Dumont JE.** Stimulation of thyroid metabolism by thyrotropin, cyclic 3′:5′-AMP, dibutyryl cyclic 3′:5′-AMP and prostaglandin E1. *Eur J Biochem* 8: 26–32, 1969.
51. **Rothberg KG, Heuser JE, Donzell WC, Ying YS, Glenney JR, Anderson RG.** Caveolin, a protein component of caveolae membrane coats. *Cell* 68: 673–682, 1992.
52. **Ruf J, Toubert ME, Czarnocka B, Durand-Gorde JM, Ferrand M, Carayon P.** Relationship between immunological structure and biochemical properties of human thyroid peroxidase. *Endocrinology* 125: 1211–1218, 1989.
53. **Simons K, Ikonen E.** Functional rafts in cell membranes. *Nature* 387: 569–572, 1997.
54. **Song Y, Driessens N, Costa M, De D, X, Detours V, Corvilain B, Maenhaut C, Miot F, Van Sande J, Many MC, Dumont JE.** Roles of hydrogen peroxide in thyroid physiology and disease. *J Clin Endocrinol Metab* 92: 3764–3773, 2007.
55. **Trushina E, Du CJ, Parisi J, McMurray CT.** Neurological abnormalities in caveolin-1 knock out mice. *Behav Brain Res* 172: 24–32, 2006.
56. **Unger J, Boeynaems JM, Van Herle A, Van Sande J, Rocmans P, Mockel J.** In vitro nonbutanol-extractable iodine release in dog thyroid. *Endocrinology* 105: 225–231, 1979.
57. **Wang MX, Wei A, Yuan J, Clippe A, Bernard A, Knoops B, Murrell GA.** Antioxidant enzyme peroxiredoxin 5 is upregulated in degenerative human tendon. *Biochem Biophys Res Commun* 284: 667–673, 2001.
58. **Wattel S, Mircescu H, Venet D, Burniat A, Franc B, Frank S, Andry G, Van Sande J, Rocmans P, Dumont JE, Detours V, Maenhaut C.** Gene expression in thyroid autonomous adenomas provides insight into their physiopathology. *Oncogene* 24: 6902–6916, 2005.
59. **Wikstrom L, Johansson C, Salto C, Barlow C, Campos BA, Baas F, Forrest D, Thoren P, Vennstrom B.** Abnormal heart rate and body temperature in mice lacking thyroid hormone receptor alpha 1. *EMBO J* 17: 455–461, 1998 .
60. **Wyse BD, Prior IA, Qian H, Morrow IC, Nixon S, Muncke C, Kurzchalia TV, Thomas WG, Parton RG, Hancock JF.** Caveolin interacts with the angiotensin II type 1 receptor during exocytic transport but not at the plasma membrane. *J Biol Chem* 278: 23738–23746, 2003.
61. **Yamada E.** The fine structure of the gall bladder epithelium of the mouse. *J Biophys Biochem Cytol* 1: 445–458, 1955.
62. **Zuo L, Ushio-Fukai M, Ikeda S, Hilenski L, Patrushev N, Alexander RW.** Caveolin-1 is essential for activation of rac1 and NAD(P)H oxidase after angiotensin II type 1 receptor stimulation in vascular smooth muscle cells. Role in redox signaling and vascular hypertrophy. *Arterioscler Thromb Vasc Biol* 25: 1824–1830 2005.